Fragile X Mental Retardation Protein (FMRP) controls diacylglycerol kinase activity in neurons

Ricardos Tabet[a,b,c,d], Enora Moutin[e], Jérôme A. J. Becker[a,b,c,d,1], Dimitri Heintz[f], Laetitia Fouillen[g], Eric Flatter[a,b,c,d], Wojciech Krężel[a,b,c,d], Violaine Alunni[a,b,c,d], Pascale Koebel[a,b,c,d], Doulaye Dembélé[a,b,c,d], Flora Tassone[h], Barbara Bardoni[i], Jean-Louis Mandel[a,b,c,d,j], Nicolas Vitale[k], Dominique Muller[e,2], Julie Le Merrer[a,b,c,d,1], and Hervé Moine[a,b,c,d,3]

[a]Institut de Génétique et de Biologie Moléculaire et Cellulaire, 67404 Illkirch, France; [b]Centre National de la Recherche Scientifique, UMR 7104, 67404 Illkirch, France; [c]Institut National de la Santé et de la Recherche Médicale, U964, 67404 Illkirch, France; [d]Université de Strasbourg, 67000 Strasbourg, France; [e]Department of Basic Neuroscience, University of Geneva, 1211 Geneva 4, Switzerland; [f]Institut de Biologie Moléculaire des Plantes, Plateforme Métabolomique, Unité Propre de Recherche (UPR) 2357 CNRS, Université de Strasbourg, 67082 Strasbourg, France; [g]Laboratoire de Biogènese Membranaire; UMR 5200 CNRS, Plateforme Métabolome, Université de Bordeaux, 33140 Villenave D'Ornon, France; [h]Medical Investigation of Neurodevelopmental Disorders Institute, University of California Davis Medical Center, Sacramento, CA 95817; [i]CNRS UMR 7275, Institute of Molecular and Cellular Pharmacology, University of Nice Sophia-Antipolis, CNRS Laboratoire International Associé (LIA) Neogenex, 06560 Valbonne, France; [j]Collège de France, 75005 Paris, France; and [k]Institut des Neurosciences Cellulaires et Intégratives, UPR3212 CNRS, Université de Strasbourg, 67084 Strasbourg, France

Edited by Don W. Cleveland, University of California, San Diego, La Jolla, CA, and approved April 26, 2016 (received for review November 27, 2015)

Fragile X syndrome (FXS) is caused by the absence of the Fragile X Mental Retardation Protein (FMRP) in neurons. In the mouse, the lack of FMRP is associated with an excessive translation of hundreds of neuronal proteins, notably including postsynaptic proteins. This local protein synthesis deregulation is proposed to underlie the observed defects of glutamatergic synapse maturation and function and to affect preferentially the hundreds of mRNA species that were reported to bind to FMRP. How FMRP impacts synaptic protein translation and which mRNAs are most important for the pathology remain unclear. Here we show by cross-linking immunoprecipitation in cortical neurons that FMRP is mostly associated with one unique mRNA: diacylglycerol kinase kappa (Dgkκ), a master regulator that controls the switch between diacylglycerol and phosphatidic acid signaling pathways. The absence of FMRP in neurons abolishes group 1 metabotropic glutamate receptor-dependent DGK activity combined with a loss of Dgkκ expression. The reduction of Dgkκ in neurons is sufficient to cause dendritic spine abnormalities, synaptic plasticity alterations, and behavior disorders similar to those observed in the FXS mouse model. Overexpression of Dgkκ in neurons is able to rescue the dendritic spine defects of the Fragile X Mental Retardation 1 gene KO neurons. Together, these data suggest that Dgkκ deregulation contributes to FXS pathology and support a model where FMRP, by controlling the translation of Dgkκ, indirectly controls synaptic proteins translation and membrane properties by impacting lipid signaling in dendritic spine.

fragile X syndrome | FMRP | diacylglycerol kinase | CLIP | translation control

Fragile X syndrome (FXS), the most common cause of inherited intellectual disability and autism, is due to the transcriptional inactivation of the Fragile X Mental Retardation 1 gene (*FMR1*) (1, 2). The *FMR1* knockout (KO) mouse ($Fmr1^{-/y}$) replicates phenotypes similar to human symptoms—including autistic-like behaviors, cognitive deficits, and hyperactivity—as well as abnormal dendritic spine morphology (3). *FMR1* encodes Fragile X Mental Retardation Protein (FMRP), an RNA-binding protein associated to polyribosomes and involved in the translational control of mRNAs important for synaptic plasticity (4). Consistent with a posttranscriptional function, the absence of FMRP in $Fmr1^{-/y}$ mouse causes abnormal signaling of group 1 metabotropic glutamate receptors (mGluRI), leading to several forms of abnormal synaptic plasticity that rely on protein translation (5, 6). Protein expression analyses confirmed a role of FMRP in neuronal translational control (7), but the extent of this control remains unclear. Although several studies focusing on individual mRNA targets (e.g., *Fmr1*, *Map1b*, *Psd95*, *App*, etc.) suggest specific control by FMRP (2), studies of global translation, including in vivo labeling in the $Fmr1^{-/y}$ mouse (8), showed thousands of neuronal proteins deregulated in the absence of FMRP, pointing toward a general translational derepression. Studies seeking to identify the transcripts controlled by FMRP identified candidate mRNAs numbering in the hundreds to thousands (9–13). The lack of obvious overlap between several of these candidate lists calls into question the RNA binding specificity of FMRP (13). How FMRP controls the translation of hundreds of distinct proteins, whether by direct mRNA binding or in an mRNA-independent manner [e.g., through its direct binding with the ribosome (14)], is still unclear. With these hundreds of potential target mRNAs, another key question still awaits an answer: Are there specific mRNAs whose deregulation matters the most for the pathology?

Cross-linking immunoprecipitation (CLIP) is a powerful technique to capture the cognate targets of RNA binding proteins (15). Intriguingly, prior CLIPs on FMRP showed rather modest overlaps

Significance

Fragile X syndrome (FXS), the most frequent form of inherited intellectual disability, is caused by the absence of the protein Fragile X Mental Retardation Protein (FMRP) in neurons. In the absence of FMRP, the translation of a high number of mRNAs is increased in glutamatergic synapses, leading to abnormal synaptic function. It is unclear whether FMRP individually controls each of these mRNAs and whether some mRNAs are more important for the pathology. This study shows that FMRP mostly associates with and controls one main mRNA target in neurons, diacylglycerol kinase kappa (Dgkκ), a master regulator that controls two key signaling pathways activating protein synthesis. The deregulation of Dgkκ could account for many of the symptoms associated with FXS and could represent a novel therapeutic target.

Author contributions: J.A.J.B., N.V., D.M., J.L.M., and H.M. designed research; R.T., E.M., J.A.J.B., D.H., L.F., E.F., W.K., V.A., P.K., N.V., D.M., J.L.M., and H.M. performed research; W.K., D.D., F.T., B.B., and N.V. contributed new reagents/analytic tools; R.T., E.M., J.A.J.B., D.H., L.F., J.-L.M., N.V., D.M., J.L.M., and H.M. analyzed data; H.M. supervised the study; and R.T., E.M., J.A.J.B., N.V., J.L.M., and H.M. wrote the paper.

The authors declare no conflict of interest.

This article is a PNAS Direct Submission.

Data deposition: The data reported in this paper have been deposited in the Gene Expression Omnibus (GEO) database, www.ncbi.nlm.nih.gov/geo (accession no. GSE51649).

See Commentary on page 7009.

[1]Present address: Physiologie de la Reproduction et des Comportements, INRA, UMR0085, CNRS, UMR7247, Université François Rabelais, 37380 Nouzilly, France.

[2]Deceased April 29, 2015.

[3]To whom correspondence should be addressed. Email: moine@igbmc.fr.

This article contains supporting information online at www.pnas.org/lookup/suppl/doi:10.1073/pnas.1522631113/-/DCSupplemental.

(13). Whether influenced by the choice of starting material (brain extracts vs. nonneuronal proliferating cells) or the experimental construction (endogenous vs. tagged protein; whole cell content vs. subcellular fraction; etc.), these studies focused more on determining the binding motives rather than on identifying all of the mRNA species bound to FMRP. Using a CLIP strategy in mouse cortical neurons that preserves the integrity of mRNAs and comparing the RNAs immunoprecipitated in *Fmr1*$^{+/y}$ vs. *Fmr1*$^{-/y}$ extracts, we find that FMRP mostly associates with a single mRNA species. This transcript encodes diacylglycerol kinase kappa (Dgkκ), a member of the master regulator DGK family. Dgkκ acts as a spatiotemporal switch between the diacylglycerol (DAG) and phosphatidic acid (PA) signaling pathways, downstream of mGluRI and upstream of general translation activation control. Our data reveal that the deregulation of mGluRI-dependent DGK activity is a substantial contributor to FXS symptoms observed in the mouse model, one that can explain the paradoxical global protein synthesis deregulation observed in *Fmr1*$^{-/y}$ neurons.

Results

FMRP Associates with One Main mRNA Species in Mouse Cortical Neurons, *Dgkκ* mRNA. To identify the mRNAs associated with FMRP, we performed a CLIP approach on dissociated cortical neurons. To control for cross-reaction of anti-FMRP antibodies to other RNA-binding proteins (such as the FMRP paralogs FXR1P or FXR2P), we performed the CLIP both on neurons from wild-type (*Fmr1*$^{+/y}$) and *Fmr1* KO (*Fmr1*$^{-/y}$) mice (Fig. S1 *A*–*C*). (All raw data of the figures can be provided upon request.) The H120 polyclonal anti-FMRP antibody was used based on its ability to efficiently immunoprecipitate FMRP (Fig. S1*D*) together with several mRNAs considered as validated FMRP targets (e.g., *Dlg4*, *Map1b*, *CamK2a*, and *Arc*), in comparison with mRNAs considered as non-FMRP targets (*PO*, *Glrb*, *ActB*, and *28S*) (Fig. S1*E*). Because prior CLIP-sequencing studies did not identify the G-quadruplex motif, the highest affinity binding motif known for FMRP (11, 12), we kept the RNAs intact to perform random reverse transcription followed by microarray so that GC-rich or other sequencing-resistant motives would not impede the mRNA identification. Aside from *Fmr1* itself (whose mRNA expression is prevented by the KO design), only two genes showed significantly altered expression when comparing the total RNA levels from *Fmr1*$^{+/y}$ and *Fmr1*$^{-/y}$ neurons: *Apol7c* and *Tmsb15l* (Dataset S1). Both transcripts showed an approximate twofold reduction in *Fmr1*$^{-/y}$ neurons, and neither has an obvious link to FXS, indicating that a loss of FMRP has virtually no impact on the whole transcriptome profile of neurons. Among 28,853 interrogated transcripts, 596 are enriched by CLIP in *Fmr1*$^{+/y}$ compared with *Fmr1*$^{-/y}$ neurons (as scored by enrichment in *Fmr1*$^{+/y}$ compared with *Fmr1*$^{-/y}$ extracts, relative to input amounts; Fig. 1 *A* and *B*) at a *P* value ≤ 0.05 compared with 298 transcripts that are depleted (Fig. 1*A*). This difference increases exponentially with decreasing *P* value (Fig. 1*B*), confirming the FMRP specificity of the approach. More than 20% (126 of 596) of the CLIP-identified transcripts have been identified in the previous study by Darnell et al. (11) (Fig. S1*F*). Of the 596 CLIP-identified transcripts, only 7 mRNAs are enriched by more than twofold. The remaining transcripts have CLIP efficiencies that are thus mostly resulting from nonspecific binding. *Dgkκ* mRNA strikingly stands out as the sole mRNA with a CLIP efficiency well above any other mRNA. Consistent with this observation, all 27 microarray probe sets covering *Dgkκ* mRNA show a high CLIP signal, indicating that *Dgkκ* mRNA is cross-linked to FMRP as an entire 8.2-kb transcript (Fig. S1*G*). The results of the microarrays were confirmed by quantitative RT-PCR (qRT-PCR) for *Dgkκ* and 42 other RNAs, including the RNAs with next-best high CLIP score (*Tln2*, *Ppfia3*, *Ogdh*, *Apc*, etc.) and previously proposed as targets (11, 12) (*Dlg4*, *Camk2a*, *Agap2*, *Shank3*, etc.) (Fig. 1*C*). Comparison of CLIP efficiencies by microarray and by qRT-PCR for these 43 RNAs shows that *Dgkκ* is by far the mRNA most efficiently and reproducibly coimmunoprecipitated with anti-FMRP H120 in cortical neurons (Fig. 1*D*). Apart from *Dgkκ*, 10% of the other tested mRNAs (10 of 42) have CLIP efficiencies that are consistent between the microarray and qRT-PCR data. The variability in CLIP efficiency of the remaining mRNAs is probably a result of their weak interaction or cross-linking efficiency with FMRP. To control that the CLIP was not biased by the antibody used, we repeated it with validated 7G1-1 antibody (9). Again, the comparison of *Dgkκ* CLIP efficiency with that of 14 different mRNAs, including mRNAs previously established as target (*APC*, *Map1B*, *Dlg4*, etc.) as well as "negative" mRNAs (*Actb*, *28S*, etc.), shows that *Dgkκ* is the mRNA with the strongest CLIP efficiency for FMRP (Fig. S1*H*).

To determine whether the FMRP–*Dgkκ* mRNA interaction revealed by the CLIP approach was due to a cross-linking artifact, we analyzed the interaction between FMRP and *Dgkκ* mRNA by in vitro binding assays. Human His-tagged FMRP binds to a *FMR1* mRNA fragment (N19) with the highest affinity known previously (12, 16) (Fig. 2*A*). *Dgkκ* transcript easily displaces *FMR1* mRNA fragment N19, contrary to nonspecific RNAs (antisense *Dgkκ* transcript) or RNAs with lower CLIP efficiency (*Dlg4*) (Fig. 2*A*). These data indicate that human FMRP binds to mouse *Dgkκ* mRNA with the highest affinity currently identified compared with any other transcript.

FMRP Positively Controls Dgkκ Translation. We developed a polyclonal antibody against Dgkκ and validated it using *Dgkκ* expressing vector in COS cells (Fig. S2*A*). Remarkably, in dissociated cortical neurons [7 days in vitro (DIV)], the main protein product detected by the antibody is severely reduced in absence of FMRP (Fig. 2*B*). These data suggest that FMRP is required for the effective translation of *Dgkκ* mRNA. To confirm an impact of the absence of FMRP on Dgkκ translation in brain, we analyzed the profile of *Dgkκ* mRNA in mouse brain polysomes using qRT-PCR. In *Fmr1*$^{+/y}$ brain extracts, *Dgkκ* mRNA is primarily associated with light and heavy polysomes, consistent with a normal translation rate (Fig. 2*C*). By contrast, in *Fmr1*$^{-/y}$ extracts, *Dgkκ* mRNA is less present in polysomal fractions and more present in monosomal fractions, whereas the distribution of other tested mRNAs *Dlg4* and *Map1b* is not altered. These data are in agreement with an impairment of Dgkκ translation in absence of FMRP.

DGK Activity Is Deregulated in the Absence of FMRP. Dgkκ converts DAG into PA (Fig. 2*D*). We assessed PA and DAG levels in dissociated cortical neurons using a liquid chromatography coupled to tandem mass spectrometry (LC-MS/MS) lipidomics approach. PA profiling using multiple reaction monitoring (MRM) MS/MS mode revealed three major PA species (Fig. S2*C*), namely, 36:1, 38:1, and 38:2. PA level is maintained at low levels in cells by the activity of potent lipid phosphate phosphohydrolase (17), but increases rapidly in neurons on activation of mGluRs and its G protein-coupled phospholipase C, immediately upstream of DGKs (18). Indeed, a brief application of group 1 mGluR (mGluRI) agonists (*S*)-3,5-dihydroxyphenylglycine (DHPG; 10 min; 100 μM) (Fig. S2*D*) or L-quisqualic acid (Quis; 10 min; 5 μM) (Fig. 2*E*) increased 36:1, 38:1, and 38:2 PAs by 40% ± 4%, 18% ± 5%, and 40% ± 6%, respectively. Quis has a more robust action than DHPG as indicated by ERK1/2 phosphorylation (Fig. S2*B*) and was chosen for the rest of the experiments. The mGluR-dependent increase of PAs depends on DGK activity because a pretreatment with DGK-specific inhibitors R59022 and R59949 (19) prevents the effect (Fig. 2*E*, Quis+R). In unstimulated *Fmr1*$^{-/y}$ neurons, PA levels are not significantly different from in *Fmr1*$^{+/y}$ neurons (Fig. 2*F*). In Quis-stimulated *Fmr1*$^{-/y}$ neurons, the increase of PA seen in *Fmr1*$^{+/y}$ neurons was lost (Fig. 2*F*), indicating that the Quis-dependent DGK activation requires FMRP. To determine whether the PA synthesis defect could be due to an alteration upstream of the DGK activity, we analyzed DAG levels in *Fmr1*$^{+/y}$ and *Fmr1*$^{-/y}$ neurons (Fig. 2*G*). In unstimulated neurons, an increase of 60.8% ± 10% of total DAG was observed in the *Fmr1*$^{-/y}$ compared

with *Fmr1*$^{+/y}$ neurons. This increase affected most major DAG species (Fig. S2*E*). Upon Quis stimulation, a similar increase of total DAG level in *Fmr1*$^{+/y}$ and *Fmr1*$^{-/y}$ neurons indicated that the absence of FMRP does not impair DAG synthesis. Together, these data indicate that the defect of Quis-dependent PA synthesis and the excess of DAG observed in *Fmr1*$^{-/y}$ neurons is due to a loss of DGK activity. To test whether a loss of DGK activity could be detected in humans, we analyzed postmortem cerebellar extracts of

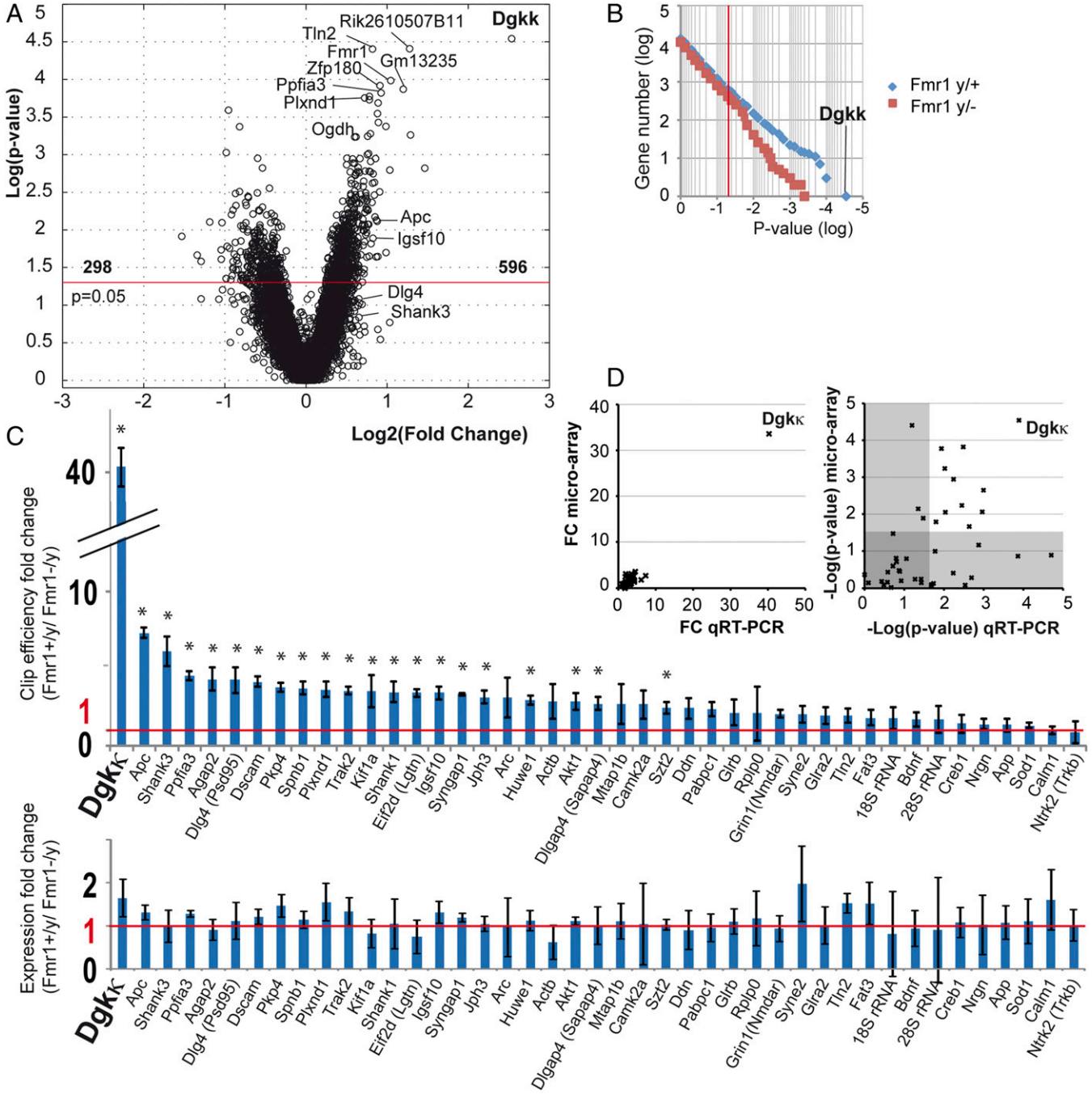

Fig. 1. FMRP mostly targets *Dgkκ* mRNA in murine cortical neurons. (*A*) Volcano plot representation of the FMRP CLIP-microarray results. The *x* axis is log2 of fold change of average intensity for each individual dataset (AI) from *Fmr1*$^{+/y}$ immunoprecipitated samples relative to *Fmr1*$^{+/y}$ total RNA input compared with *Fmr1*$^{-/y}$ immunoprecipitated samples relative to *Fmr1*$^{-/y}$ total RNA input [i.e., Log2([AI$^{\text{Wt CLIP}}$/AI$^{\text{Wt Input}}$]/[AI$^{\text{KO CLIP}}$/AI$^{\text{KO Input}}$])]. The *y* axis is –log(*P* value) with *P* value determined by using the significance analysis of microarrays test (*Materials and Methods*) with $n = 5$ (i.e., one microarray per independent CLIP experiment per biological replicate). The name of a few mRNAs with high *P* value or previously proposed as targets is given, and the arbitrary 0.05 *P* value thresholds with corresponding number of genes are shown. (*B*) Representation of CLIP-identified transcripts number as a function of the *P* value determined as in *A*. (*C*, *Upper*) qRT-PCR validation of immunoprecipitated mRNAs. Data are fold changes of CLIP efficiency of 43 RNAs chosen among the best immunoprecipitated mRNAs (*Dgkκ*, *Tln2*, *Ppfia3*, *Ogdh*, *Apc*, etc.) or previously proposed as targets (*Dlg4*, *Camk2a*, *Agap2*, *Shank3*, etc.) or non-FMRP targets (*RplP0*, *Actb*, *18S*, and *28S*) determined by qRT-PCR using the ΔΔCT method ([CT$^{\text{Wt CLIP}}$ – CT$^{\text{Wt Input}}$] – [CT$^{\text{KO CLIP}}$ – CT$^{\text{KO Input}}$]). Data are means ± SD. *$P \leq 0.05$ (unpaired *t* test, $n = 4$ biological replicates). (*C*, *Lower*) Absence of differential expression of the 43 RNAs between *Fmr1*$^{+/y}$ and *Fmr1*$^{-/y}$ neuron extracts. Fold change of expression was calculated with ΔΔCT method with *Rplp0* or *ActB* as normalizer. (*D*) Scatter plot representation of the fold change of clip efficiency of the 43 RNAs as in *C*, determined by microarray vs. by qRT-PCR (*Left*) and of their *P* value (*Right*); gray zones indicate >0.05 *P* value.

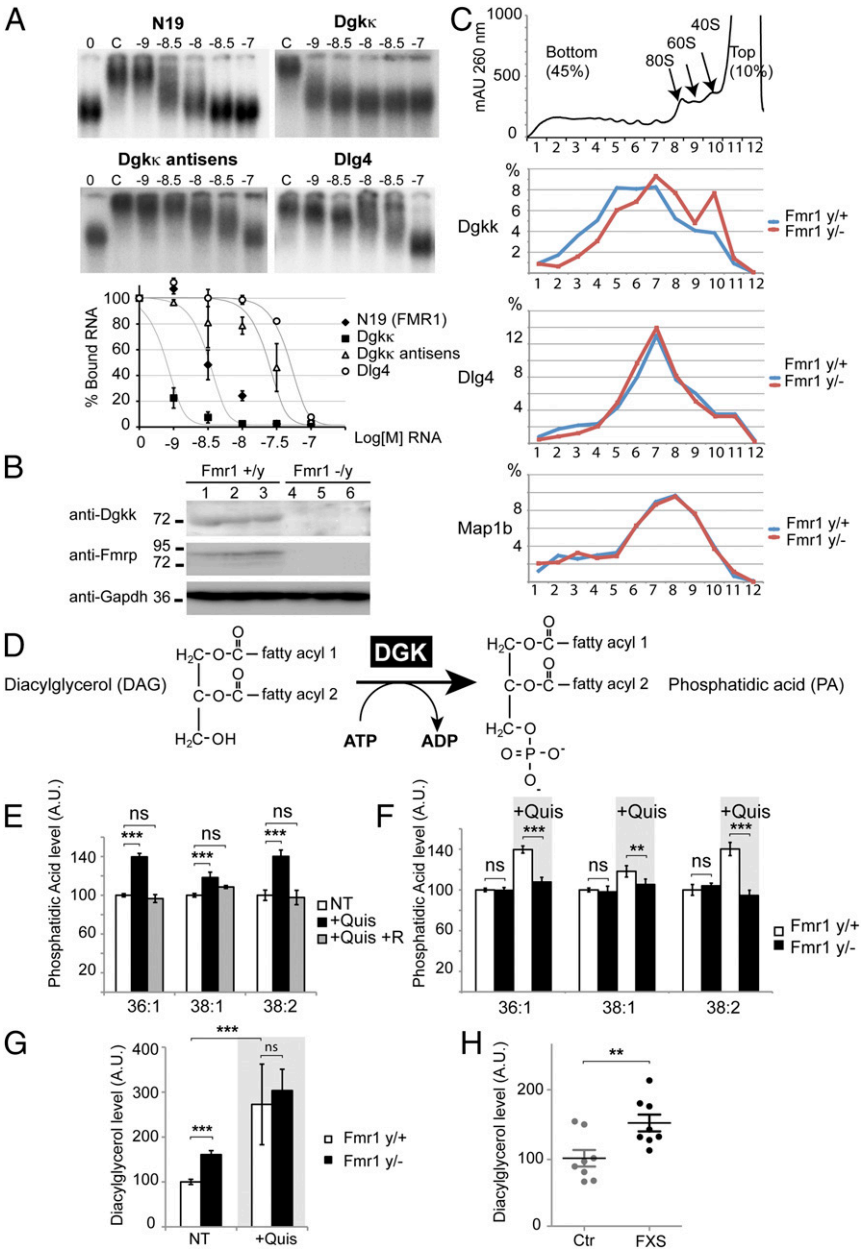

Fig. 2. FMRP positively controls Dgkκ expression. (*A*) Gel shift assay competition to determine the relative binding strength of FMRP for *Dgkκ* mRNA. ^{32}P-labeled *Fmr1* N19 mRNA fragment was incubated with His-FMRP Iso7 (0.1 pmol) in the presence of increasing concentrations of indicated unlabeled competitor RNAs. Lane 0, control without protein; lane C, control without competitor RNA; numbers are log of competitor RNA concentrations. The graph depicts the fraction of bound labeled N19 RNA plotted against unlabeled competitor RNA concentration. Data are means ± SD, $n = 3$. (*B*) Western blot analysis with indicated primary antibodies in cortical neuron extracts. Lanes 1–6 indicate biological replicates for the corresponding genotypes. The molecular mass of protein markers is indicated (kDa). (*C*) Brain polysome profile from 10-d-old mice shows decreased ribosome loading for *Dgkκ* mRNA in the absence of FMRP. qRT-PCR analysis (expressed as percent of total fractions) reveals an increased amount of *Dgkκ* mRNA in monosomal fractions and decreased amount in polysomal fractions in *Fmr1*$^{-/y}$ compared with *Fmr1*$^{+/y}$ brain extracts, but no major change in *Dlg-4* or *Map1b* mRNAs (data are means of two biological replicates with two technical replicates). (*D*) DGKs convert DAG into PA. (*E*) Bar diagram showing relative PA levels in dissociated cortical neurons. Measurements were made by LC-MS/MS, MRM mode on total lipid extracts from *Fmr1*$^{+/y}$ and *Fmr1*$^{-/y}$ murine cortical neurons (8 DIV). The level of the three major PAs (36:1, 38:1, and 38:2) is shown in basal conditions (NT), after mGluRI activation with Quis treatment, 5 μM 10 min (+Quis), and after 15 min DGK inhibitors 3 μM R59022 and 0.2 μM R59949 at 6 μM prior Quis 5μM 10 min (+Quis+R). Values are relative to the untreated samples. A.U., arbitrary units. $n = 5$. ***$P < 0.001$ (unpaired *t* test); ns, nonsignificant. Data are means ± SD. (*F*) Bar diagram showing relative PA levels in untreated *Fmr1*$^{+/y}$ and *Fmr1*$^{-/y}$ cortical neurons and after treatment with Quis 5 μM 10 min (+Quis). ***$P < 0.001$, **$P < 0.01$; $n = 5$. (*G*) Bar diagram showing relative total DAG levels in cortical neurons. Measurements were made with LC-MS/MS on total lipid extracts from *Fmr1*$^{+/y}$ and *Fmr1*$^{-/y}$ cortical neurons (8 DIV) in basal conditions (NT) and after Quis treatment 5 μM 10 min (+Quis). ***$P < 0.001$, $n \geq 3$. (*H*) Bar diagram showing relative total DAG levels in normal (ctr) and fragile X (FXS) human postmortem cerebellum extracts. Measurements were made as in *G*. **$P < 0.01$ (unpaired *t* test, $n = 4$ biological replicates with technical replicates).

FXS patients, the cerebellum being a region of the brain affected by FXS (20). Remarkably, an excess of DAG is observed in the FXS compared with the nonaffected samples (Fig. 2*H*).

Dgkκ Loss of Function Reproduces FXS-Like Phenotype. *Dgkκ* mRNA is expressed throughout the brain (Fig. S3*A*), but its involvement in synaptic plasticity was unknown. We focused on the

well-characterized CA1 region of mouse hippocampus. We performed *Dgkκ* silencing in organotypic slices with a validated shRNA (Fig. S3 *B–D*). We examined the effect of *Dgkκ* silencing on long-term potentiation (LTP) and long-term depression (LTD), two forms of synaptic plasticity that are altered in *Fmr1*$^{-/y}$ mice (5, 21, 22). Theta burst stimulation (TBS)-induced LTP at Schaffer collateral-CA1 region was reduced with shRNA–*Dgkκ* (112% ± 3% at 30–40 min, instead of 135% ± 6% with shRNA–scramble) (Fig. 3*A*), whereas low-frequency stimulation-induced LTD was increased (83% ± 3% at 30–40 min, instead of 95% ± 3% with shRNA–scramble) (Fig. 3*B*). These data indicate that the reduction of *Dgkκ* in CA1 neurons induces synaptic plasticity alterations. Remarkably, these alterations are similar to the one observed in FXS mouse model (6). Approximately 50% of patients with FXS also carry an autism diagnosis, and recent research on hallmark autistic symptoms point toward striatal dysfunction (23, 24). To test whether *Dgkκ* loss of function could contribute to FXS phenotype, AAV9-delivered shRNA–*Dgkκ* was injected bilaterally into the striatum of wild-type mice. Injected mice were submitted for behavioral testing to assess autism-like behaviors, cognitive impairments, and hyperactivity, the most frequent FXS phenotypes. Four weeks after injection, shRNA expression was broadly spread across the striatal regions (Fig. 4*A* and Fig. S4 *A–C*). Consistent with autistic phenotype, animals expressing shRNA–*Dgkκ* show deficient social interaction, altered nest-building behavior, and spontaneous motor stereotypies compared with mice expressing shRNA–*scramble* (Fig. 4 *B–D* and Fig. S4 *D–G*), all striatal-dependent symptoms observed in *Fmr1*$^{-/y}$ mice (25–28). Stereotypic behavior is indicated by an enhanced learning on the accelerating rotarod (24), mainly at late stages of learning (Fig. 4*E*). In the novel object recognition (NOR) test, shRNA–*Dgkκ*-expressing mice showed repetitive patterns of exploration, evocative of cognitive inflexibility, but no detectable memory impairment (Fig. 4*F*). The absence of memory impairment in these animals, in contrast with *Fmr1*$^{-/y}$ mice, is a likely consequence of a striatal-centered shRNA expression, sparing cortices and hippocampus. Finally, shRNA–*Dgkκ*-expressing animals were hyperactive, crossing quadrants more frequently during NOR testing and traveling longer distances in activity boxes (Fig. 4*G*). Together, these data indicate that animals with striatal silencing of *Dgkκ* mimic autistic and hyperactivity symptoms and recapitulate the core neurologic phenotypes observed in *Fmr1*$^{-/y}$ mice.

Finally, we examined the impact of *Dgkκ* loss of function on dendritic spine morphology and dynamics. *Dgkκ* silencing in the CA1 region of mouse hippocampus organotypic slices caused a strong increase of abnormally long and multiheaded spines and a marked decrease of the proportion of mature spines (Fig. 5 *A–E*), whereas spine density remained unchanged (Fig. 5*C*). Additionally, there was a significant increase of spine turnover, as indicated by the increased rate of spine formation and elimination, associated with spine instability in *Dgkκ* silenced neurons (Fig. S5 *A–C*). These data indicate that *Dgkκ* is necessary for spine maturation and maintenance and that its loss leads to structural defects similar to those previously observed in the *Fmr1*$^{-/y}$ mice (29, 30). To establish a functional link between Dgkκ and FMRP, we tested whether the overexpression of Dgkκ within *Fmr1*$^{-/y}$ neurons could rescue the dendritic spine phenotype. Remarkably, *Fmr1*$^{-/y}$ neurons transfected with plasmid expressing *Dgkκ* had their spine defects corrected (Fig. 5 *A–F*, *Fmr1*$^{-/y}$+Dgkκ), indicating that *Dgkκ* overexpression is able to compensate for the lack of FMRP.

Discussion

Based on a CLIP analysis of FMRP-bound mRNAs, we provide evidence that *Dgkκ* mRNA is a primary target of FMRP in cortical neurons. Surprisingly, although previous analyses have identified hundreds of potential FMRP-binding mRNA candidates, *Dgkκ* mRNA was not identified (9–12). Although we have no definitive

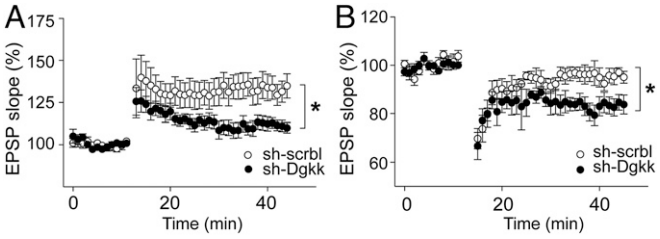

Fig. 3. Synaptic alterations induced by interference with *Dgkκ* expression. (*A*) Decrease in LTP in slice cultures infected with shRNA–*Dgkκ* ($n = 7$) vs. shRNA–*scramble* ($n = 6$) expressing AAV viruses. *$P < 0.05$ (two-way ANOVA). (*B*) Increase in LTD in slice cultures infected with shRNA–*Dgkκ* ($n = 7$) vs. shRNA–*scramble* ($n = 6$) expressing AAV viruses. *$P < 0.05$ (two-way ANOVA).

answer as to why *Dgkκ* was not discovered before, several explanations can be proposed. First, it should be noted that *Dgkκ* was identified in 2005 (31); thus, it could not have been identified by initial microarray studies. A second factor is the starting biological material. Although we used pure neuron cultures, Ascano et al. (12) performed CLIP in kidney cells where *Dgkκ* may have been missed easily because its expression is 100-fold lower in kidney than in neuronal tissues (Fig. S3*E*). Darnell et al. performed CLIP on brain homogenate where Dgkκ should have appeared. However, whether Dgkκ CLIP efficiency is lower in brain homogenates compared with neuron cultures or whether *Dgkκ* was lost during the purification step of brain polyribosomes (performed to reduce the high complexity of whole brain extracted material) remains to be determined. Another factor is the bioinformatics treatment of data because *Dgkκ* suffers from database annotation problems. Human *DGKκ* is annotated as a noncoding gene in genome build 37 (GRCh37) (this error has been corrected in GRCh38), and mouse Dgkκ lacks exon 1 (noted as unsequenced). These problems may have screened out *Dgkκ* during the bioinformatics analyses. Finally, other factors may have been critical for identification of *Dgkκ*. First, as explained in results, we kept mRNAs intact in cases where structured regions are difficult to amplify. Second, we normalized mRNA targets both to the input (to avoid problem of expression level) and to the signal from *Fmr1*$^{-/y}$ littermates (to reduce the noise of unspecific binding). Finally, we quantified results both by microarrays and qPCR.

Our CLIP also identified another 595 mRNAs as significantly associated with FMRP (Fig. 1*A*). The lower and more variable CLIP efficiency of most of these mRNAs compared with *Dgkκ* suggests that they are occasional rather than bona fide interactors.

How FMRP specifically interacts with *Dgkκ* mRNA remains to be defined. None of the previously proposed motives bound by FMRP could be evidenced in Dgkκ (e.g., *Dgkκ* does not contain motifs that would readily establish a G-quadruplex structure). However, *Dgkκ* mRNA is highly conserved from mouse to human, with 77% nucleotide identity for coding regions and 68% for UTRs. Furthermore, the FMRP binding site is apparently sufficiently conserved to allow cross-species interaction between human FMRP and mouse mRNA (Fig. 2*A*). It will be important to define whether a specific RNA motif exists in *Dgkκ* mRNA specifying FMRP binding. In contrast with most of its previous characterized targets, FMRP positively controls Dgkκ translation (Fig. 2 *B* and *C*). How FMRP can stimulate Dgkκ translation is the next pending question. The alleviation of a miRNA repression, such as the one identified for FXR1, is a possibility (32). Upon identification of *Dgkκ* mRNA as a main interactor of FMRP, we focused our analysis on the biological significance of a *Dgkκ* deregulation in FXS *Fmr1*$^{-/y}$ mouse model. Dgkκ is a member of the DGK isozymes, master regulators of the balance between DAG and PA signaling (31). Several DGKs have been shown to be involved in structural and synaptic plasticity control (33–36), but no data were available on *Dgkκ* neuronal function. We identified

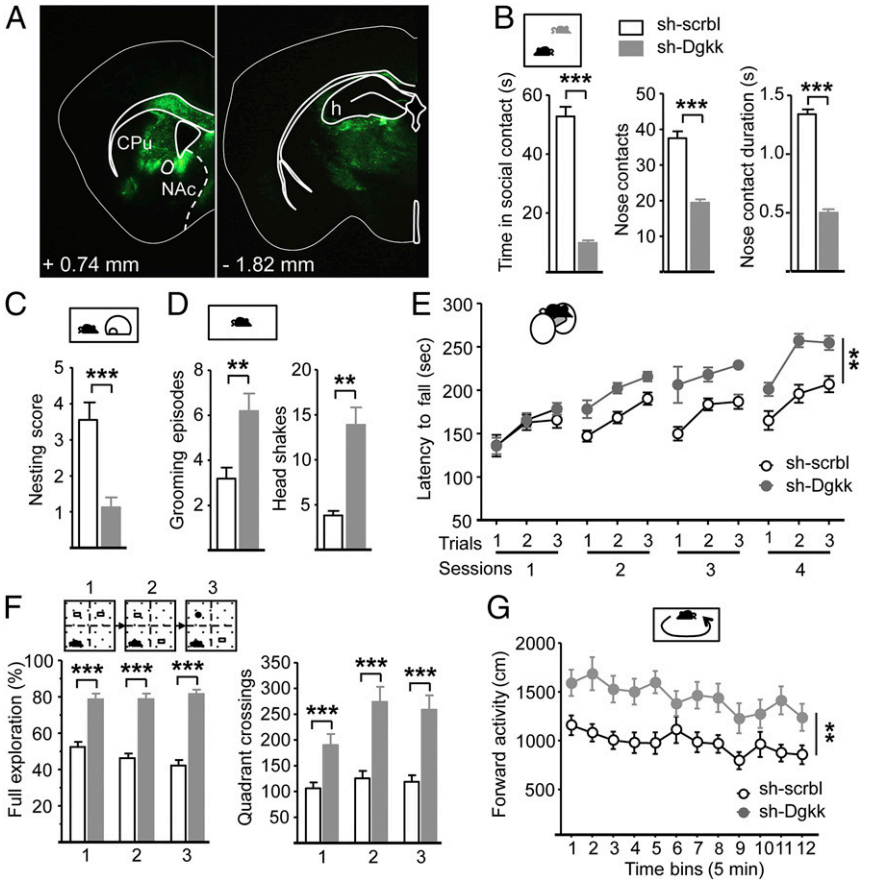

Fig. 4. Interference with *Dgkκ* expression in the striatum leads to FXS-like behavior. (*A*) Representative distribution of GFP 4 wk after stereotaxic AAV injection shows striatum-centered shRNA expression, sparing cortices and hippocampus. Coordinates refer to Bregma. CPu, caudate putamen; h, hippocampus; NAc, nucleus accumbens. (*B*) Mice expressing shRNA–*Dgkκ* (sh-*Dgkκ*) show decreased time spent in social contact, due notably to diminished number and duration of nose contacts compared with shRNA–*scramble* (sh-*scrbl*)-expressing mice (n = 16 per AAV treatment). ***$P < 0.001$ (one-way ANOVA). (*C*) Mice expressing shRNA–*Dgkκ* (sh-*Dgkκ*) fail to build proper nests. ***$P < 0.001$ (Kruskal–Wallis ANOVA). (*D*) Mice expressing shRNA–*Dgkκ* (sh-*Dgkκ*) display spontaneous stereotypic grooming episodes and head shakes. **$P < 0.01$; (one-way ANOVA). (*E* and *F*) Consistent with stereotyped behavior, sh-*Dgkκ*–injected animals show facilitated motor skill learning on the accelerated rotarod (*E*) and repetitive patterns of exploration in the NOR test, associated with increased locomotor activity as measured by the number of quadrant crossings (*F*). **$P < 0.01$ (*E*; three-way repeated measure ANOVA); ***$P < 0.001$ (*F*; two-way repeated measure ANOVA with Newman–Keules posttest). (*G*) Hyperactivity is confirmed in activity boxes, where mice bearing a striatal knockdown of *Dgkκ* travel a longer distance over 60 min compared with shRNA–*scramble*-expressing animals. **$P < 0.01$ (two-way repeated-measure ANOVA). Data are means ± SEM.

that the absence of FMRP leads to the deregulation of mGluRI-dependent DGK activity, causing perturbations in the balance between its substrate, DAG, and its product, PA. These two second-messengers signal via many pathways in a spatiotemporally coordinated manner. DAG signals trafficking, secretion, and cytoskeletal reorganization by binding and activating C1 domain-containing proteins in neuronal and immune tissues. These proteins include PKC isozymes, PKD, chimaerins, Unc13, and RasGRP (37, 38). PA signals cell growth by interacting with many effectors (e.g., mTOR, PAK1, PIP5K, PKCε, sphingosine kinase, Raf1, etc.). Both DAG and PA trigger general protein translation through the allosteric activation of their many effectors; their physiologic concentrations are thus critical for normal protein translational control.

We showed that DAG level is increased in nonstimulated *Fmr1*$^{-/y}$ neurons, as well as in human FXS cerebellum, suggesting that an excessive DAG signaling occurs in FXS. PKCa, one main DAG effector (39), has been shown to be strongly activated in *Fmr1*$^{-/y}$ mouse brain (40). One direct consequence of PKC activation in cells is an activation of general translation (41). The perturbation of DAG level could thus explain the excess of translation observed in *Fmr1*$^{-/y}$ neurons. Furthermore, PKCs have been shown to exert control over sensitization status of mGuRI-LTD by controlling the p38 MAPK pathway (42), and mGluRI-LTP in widespread areas of the brain (39). Thus, PKCs could be an important factor in FXS synaptic plasticity deregulation. We also showed that the mGluRI-dependent PA synthesis is abolished in *Fmr1*$^{-/y}$ neurons. This finding indicates a transient deficit in PA signaling. Among PA effectors, mTOR is proposed to be abnormally activated in *Fmr1*$^{-/y}$ mice (43). mTOR signaling regulates translation initiation; however, the deregulation of this pathway does not seem to be the cause of increased protein synthesis because its inhibition does not rescue the excess of translation (44). How the mTOR pathway is precisely deregulated remains unclear.

Previous observations indicated that DAG triggers dendritic spine growth and destabilization, whereas PA is spine-stabilizing, indicating that synaptic levels of DAG and PA in neurons are determinants of the dendritic spine growth and stability (45). Thus, an increase of DAG and a lack of PA are expected to produce an increase in spine growth and a defect of spine maturation. This scenario is exactly what we observed in *Fmr1*$^{-/y}$ neurons. By controlling the switch between DAG and PA signaling, DGK activity is a key regulator of spine maintenance. Remarkably, besides *Dgkκ*, nine other DGK isozymes exist, but

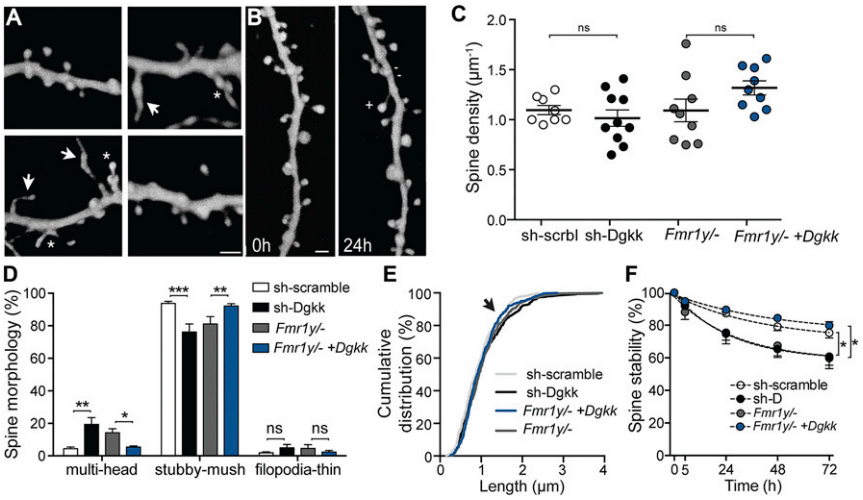

Fig. 5. Dendritic spine alterations and rescue with *Dgkκ* expression modulation. (*A*) Illustration of the changes in spine morphology in *Fmr1*$^{-/y}$ (*Left*) or *Fmr1*$^{-/y}$ (*Right*) CA1 pyramidal neurons transfected with pAAV-EGFP-shRNA-*scramble* (*Upper Left*), pAAV-EGFP-shRNA-*Dgkκ* (*Lower Left*), pAAV-EGFP (*Upper Right*), and pAAV-*Dgkκ* (*Lower Right*). Note the presence of multiheaded spines (stars) as well as very long thin spines (arrows). (Scale bar: 2 µm.) (*B*) Spine changes (new spines, +, and lost spines, −) occurring in shRNA– *scramble*-expressing pyramidal neurons. (Scale bar: 2 µm.) (*C*) Absence of changes in spine density under the four conditions. ns, not significant. (*D*) Increase in multihead spines and decrease in mature spines (stubby-mushroom) in shRNA–*Dgkκ* (sh-*Dgkκ*) ($n = 10$) vs. shRNA–*scramble* (sh-*scrbl*) transfected cells ($n = 8$) and in *Fmr1*$^{-/y}$ ($n = 9$) vs. *Fmr1*$^{-/y}$+*Dgkκ* transfected cells ($n = 8$). $^{*}P < 0.05$; $^{**}P < 0.01$; $^{***}P < 0.001$ (two-way ANOVA with Bonferroni posttest). (*E*) Distribution of spine length in shRNA–*Dgkκ* ($n = 342$ spines), shRNA–*scramble* ($n = 297$ spines), *Fmr1*$^{-/y}$ ($n = 359$ spines), and *Fmr1*$^{-/y}$+*Dgkκ* ($n = 377$ spines) transfected cells ($P = 0.13$, Kolgomorov–Smirnov test). (*F*) Decrease in spine stability over time. $^{*}P < 0.05$ (two-way ANOVA with Bonferroni posttest).

only *Dgkκ* mRNA is targeted by FMRP (Dataset S1). DGK deficiencies cause an imbalance between DAG and PA and affect cellular signaling (45). DGKs are mostly expressed in the brain, where (for those that have been studied) they influence dendritic spine morphology and synaptic plasticity (46, 47). The role of each DGK seems to differ based on its distinct localization or structure, suggesting that each has evolved specialized functions. It will be important to better define the specificity of each of these critical enzymes.

We showed that the reduction of *Dgkκ* expression in striatal areas of mouse brain reproduced the hyperactive and autistic-like behaviors similar to FXS and that the silencing of *Dgkκ* reproduces both morphological and functional spine abnormalities of *Fmr1*$^{-/y}$ mouse model. These results emphasize that *Dgkκ* is involved in the molecular basis of mGluRI-controlled mammalian synaptic plasticity, the deregulation of which accounts for several of the main neurological phenotypes found in FXS. Remarkably, the overexpression of Dgkκ within *Fmr1*$^{-/y}$ neurons rescued their spine defects, demonstrating the functional link between FMRP and Dgkκ activity.

The identification of the master-regulator *Dgkκ* as a main mRNA target of FMRP enables us to propose a novel molecular mechanism driving neuronal defects in the FXS mouse model. Instead of repressing general synaptic translation (the current proposed model), our data support a different model where FMRP is mostly dedicated to the positive control of *Dgkκ*. The defective regulation of *Dgkκ* in the absence of FMRP explains the dendritic spines and synaptic plasticity alterations observed in FXS. The increased level of DAG seen in *Fmr1*$^{-/y}$ unstimulated neurons would be a main triggering factor of the general local increase of synaptic protein synthesis seen in FXS neurons (e.g., by activating PKCs or other effectors) and the induction of abnormal spine growth. The lack of PA synthesis after mGluR activation, conversely, could be responsible for the defect in spine maturation and associated perturbations of synaptic plasticity via the failure to activate its numerous binding effectors (e.g., mTOR) and by impacting actin polymerization. Currently proposed therapeutic approaches mostly target the excess of protein synthesis observed in FXS neurons. Our present data suggest that this strategy may be insufficient: The defect of spine maturation that results from defective PA signaling and its associated lipid membrane alterations should be considered as well. DGK activity may represent a promising and novel therapeutic target.

Materials and Methods

Ethics Statement. Animal work involved in this study was conducted according to relevant national Comité National de Réflexion Ethique en Expérimentation Animale and international guidelines (86/609/CEE).

Primary Cortical Neuron Cultures. Cortices from C57BL/6J *Fmr1*$^{+/y}$ or *Fmr1*$^{-/y}$ mouse embryos (48) [embryonic day (E17.5)] were dissected in 1× PBS, 2.56 mg/mL D-glucose, 3 mg/mL BSA, and 1.16 mM $MgSO_4$; incubated for 20 min with 0.25 mg/mL trypsin and 0.08 mg/mL DNase I; and mechanically dissociated after supplementation of medium with 0.5 mg/mL trypsin soybean inhibitor, 0.08 mg of DNase I and 1.5 mM $MgSO_4$. The cells were plated on poly-L-lysine hydrobromide-coated six-well culture plates for 8 d in Neurobasal Medium (GIBCO) supplemented with B27, penicillin/streptomycin, and 0.5 µM L-glutamine.

CLIP on Primary Neurons. CLIP strategy was adapted from Ule et al. (15) with modifications for neuron cultures. Neurons from *Fmr1*$^{+/y}$ or *Fmr1*$^{-/y}$ mice grown in six-well plates for 8 DIV were gently washed with cold PBS and exposed to 254-nm UV (400 mJ/cm^2, in Stratalinker 2400) on ice. Neurons from three littermate embryos with the same genotype were pooled (constituting one biological sample) and lysed with 1 mL of lysis buffer [50 mM Tris·HCl, pH 7.4, 100 mM KCl, 1 mM $MgCl_2$, 0.1 mM $CaCl_2$, 0.1% SDS, 1% Nonidet P-40, 0.5% sodium deoxycholate, 30 U of anti-RNase (Ambion), and 10 U of DNase Turbo (Invitrogen)] for 5 min at 37 °C. Lysates were spun down at 18,000 × *g* at 4 °C, and supernatants were precleared by incubation with 50 µL of free Dynabeads protein G (Dynal) and then on 50 µL of Dynabeads protein G coupled to rabbit anti-mouse IgGs (5 µg) for 1 h each. The lysates were then incubated overnight with agitation on 50 µL of Dynabeads protein G coupled to 5 µg of anti-FMRP antibody (H-120; Santa Cruz). After immunoprecipitation, the supernatants were saved for RNA extraction (*Fmr1*$^{+/y}$ and *Fmr1*$^{-/y}$ "inputs"), and the beads were washed three times with 1 mL of high-salt washing buffer (50 mM Tris·HCl, pH 7.4, 1 M KCl, 1 mM EDTA, 1% Nonidet P-40, 0.5% sodium deoxycholate, and 0.1% SDS; 4 °C). RNAs from *Fmr1*$^{+/y}$ and *Fmr1*$^{-/y}$ neurons were recovered by treatment of the beads with 0.4 mg of proteinase K in buffer (100 mM Tris·HCl, pH 7.4,

50 mM NaCl, and 10 mM EDTA) for 20 min at 37 °C. The H120 polyclonal anti-FMRP antibody was selected among several tested antibodies (7G1.1; IC3) based on its ability to immunoprecipitate efficiently some mRNAs considered as validated FMRP targets (i.e., *Dlg4*, *Map1b*, *CamK2a*, and *Arc*) compared with mRNAs considered as non-FMRP targets (*PO*, *Glrb*, *ActB*, and *28S*) in $Fmr1^{+/y}$ compared with $Fmr1^{-/y}$ neuron extracts as quantified by qRT-PCR.

RNA Isolation and Microarray Gene Expression Analysis. RNA from $Fmr1^{+/y}$ or $Fmr1^{-/y}$ neuron inputs ($Input^{Fmr1+/y}$ and $Input^{Fmr1-/y}$) or from CLIP samples ($CLIP^{Fmr1+/y}$ and $CLIP^{Fmr1-/y}$) were extracted by phenol/chloroform (vol/vol) followed by chloroform/isoamyl alcohol (24:1) extraction and ethanol precipitated in the presence of 0.3 M sodium acetate. Quality of the RNAs was controlled by using the Bioanalyzer 2100 (Agilent). RNAs used had RNA integrity number values ≥ 6.6. CLIP and Input RNAs were then used to prepare biotinylated double-strand cDNA targets with the NuGEN Ovation Pico WTA System V2 Kit (catalog no. 3302) followed by the NuGEN Encore Biotin Module Kit (catalog no. 4200), according to manufacturer recommendations. After fragmentation and end-labeling, 2 μg of cDNAs was hybridized for 16 h at 45 °C on GeneChip Mouse Gene 1.0 ST arrays (Affymetrix) interrogating 28,853 genes (26,166 RefSeq transcripts). The chips were washed and stained in the GeneChip Fluidics Station 450 (Affymetrix) and scanned with the GeneChip Scanner 3000 7G (Affymetrix) at a resolution of 0.7 μm. Raw data (.CEL Intensity files) were extracted from the scanned images by using the Affymetrix GeneChip Command Console (Version 3.2). CEL files were further processed with Affymetrix Expression Console software (Version 1.1) to calculate probe set signal intensities using Robust Multiarray Average algorithms with default settings. On mouse Gene 1.0 ST arrays, the majority of genes are represented by one unique probe set, composed of ∼27 probes spread across the full length of the gene, giving a single signal intensity value. A minority of genes on the array are interrogated by several probe sets. For those genes, we used the median of all probe set signal intensity values as a measure of their expression. Thus, only one fold change value was calculated for each gene on the array as the ratio of the signal intensity between $Fmr1^{+/y}$ and $Fmr1^{-/y}$ conditions (FC_adjusted in Dataset S1, raw data can be accessed at www.ncbi.nlm.nih.gov/geo/query/acc.cgi?acc=GSE51649). The *P* value for probe sets signal intensity change between conditions was determined by using the Significance Analysis of Microarrays test (49) ($n = 5$ biological replicates; i.e., one microarray per independent CLIP experiment per biological replicate).

cDNA Synthesis and qRT-PCR Validation of RNAs with Best CLIP Scores. The first strand cDNA was performed with SuperScript II Reverse Transcriptase kit (Invitrogen) following manufacturer instructions. A total of 0.5 μg of RNA from inputs or one-fourth from CLIP RNAs were used with gene-specific primer mix (2 pmol each; see Table S1 for primer sequences). Primers were validated with standard dilution curve on $Fmr1^{+/y}$ RNA input before quantification of mRNA levels with a Lightcycler 480 (Roche). qRT-PCR was performed on cDNA dilutions of 1/500 for ribosomal RNA and 1/4 for other genes in the presence of 7.5-pmol primers with QuantiTect SYBR Green PCR Master Mix (Qiagen). For CLIP experiments, two technical replicates were performed for at least three biological replicates for 43 different genes. Fold change between $CLIP^{Fmr1+/y}$ and $CLIP^{Fmr1-/y}$ was determined by using the following method: $mean^2\Delta Ct\ [Ct_{IP\ WT} - Ct_{input\ WT}]/mean^2\Delta Ct\ [Ct_{IP\ KO} - Ct_{input\ KO}]$. Error rates were calculated with the following formula: $square\ root((Fmr1^{+/y}\ SD/Fmr1^{-/y}\ SD)^2 + (fold\ change)^2)$.

Brain Polyribosome Profiling. Brain from 10-d-old C57BL/6J $Fmr1^{+/y}$ or $Fmr1^{-/y}$ mouse embryos were dissected and homogenized with 10 strokes of Dounce homogenizer in 0.7 mL of ice-cold lysis buffer (50 mM Tris·HCl, pH 7.4, 100 mM KCl, 5 mM MgCl2, 1 mM DTE, 40 U/mL RNasin, and 1% Nonidet P-40). Extracts were cleared by 18,000 × *g* 4 °C centrifugation for 15 min, and supernatants were loaded on linear sucrose gradient 15–45% (wt/wt) in buffer (50 mM Tris·HCl, pH 7.4, 100 mM KCl, and 5 mM MgCl2) in SW41 tubes. Gradients were centrifuged at 36,000 rpm for 2 h at 4 °C in a Beckman SW41 rotor. Gradients were collected in 12 fractions of 1 mL by using peristaltic pump coupled to AKTA (GE) detector and collector apparatus. Fractions were precipitated with 2 volumes of cold ethanol at −20 °C. Pellets obtained after centrifugation at 20,000 × *g* for 20 min were washed with 80% cold ethanol and briefly dried and resuspended in 20 μL of water. Total RNA was extracted from each fraction by acidic phenol/chloroform (1:1 vol/vol) followed by a chloroform extraction and an ethanol precipitation. RNA was resuspended in 20 μL of water, and its quality was checked on a 10th of the material by electrophoresis in 1% agarose gel with ethidium bromide. cDNA synthesis and qRT-PCR were performed as described above.

Neuron Treatments. mGluRI agonists DHPG resuspended in DMSO (Tocris) or Quis resuspended in water (Tocris) were applied on neurons at concentrations of 100 and 5 μM, respectively, for 10 min at 37 °C at 8 DIV. DGK inhibitors R59022 (DGK Inhibitor I; Calbiochem) and R59949 (DGK Inhibitor II; Calbiochem) were applied at concentrations of 3 and 0.2 μM each for 15 min at 37 °C prior an eventual mGluRI treatment.

PA Profiling by LC–MS/MS. Neurons of 8 DIV cultures (treated or not) from a single six-well plate well were washed twice with cold PBS 1× and lysed in cell extraction buffer (FNN0011; Invitrogen) supplemented with protease inhibitors (complete protease inhibitor mixture; Roche) and PMSF (1 mM) for 30 min, on ice, with vortexing at 10-min intervals. Afterward, neuron extracts were centrifuged for 18,000 × *g* for 10 min, and proteins were quantified by the Bradford method to normalize samples. Total lipids were extracted by the method of Bligh and Dyer (50). Typically, extracts were mixed with chloroform:methanol (4:1), vortexed for 10 s, and left under agitation for 1 h at 4 °C. After 5-min centrifugation at 18,000 × *g*, organic phase was recovered and used for MS analyses. The organic phase (150 μL) was analyzed by UPLC/MS/MS (Acquity UPLC System; Waters Corp.) coupled to a Quattro Premier XE triple Quadrupole MS System; Waters Micromass). Column was a Waters Acquity UPLC BEH Amide column (2.1 mm × 100 mm, 1.7-μm particle size) together with an Acquity UPLC BEH Amide precolumn (2.1 mm × 5 mm, 1.7-μm particle size). Temperature of column oven was 28 °C, and injection volume was 3 μL. Eluents were acetonitrile, ammonium hydroxide (99.5%:0.5%) (vol/vol) (A) and acetonitrile, water, and ammonium hydroxide (80%:19.5%,0.5%) (vol/vol) (B). The flow rate was 0.4 mL/min. Elution was as follows: 93% (vol/vol) A for 2 min. The gradient was as follows (vol/vol): 93% A to 60% A in 1 min, 60% A to 50% A in 0.5 min, and 50% A to 40% A in 1.5 min. Then the composition of the mobile phase was returned to the initial conditions as follows (vol/vol): 40% A to 50% A in 2 min, 50% A to 80% A in 2.5 min, and 80% A to 93% A in 0.5 min. The 93% A was maintained during 2 min. UV spectra were recorded from 200 to 500 nm. The system was run by Mass-Lynx software (Version 4.0). The ESI source was used in positive and negative mode with a capillary voltage of 3.4 kV, RF lens at 0 V, resolution (LM1, HM1, LM2, and HM2) 15, and ion energy 1 and 2:0.5. Source and desolvation temperatures were 135 °C and 400 °C. Flow rates of nitrogen for nebulizer and desolvation were 50 and 900 L/h. Pressure of the argon collision gas was 3.0×10^{-3} mbar. Full-scan, selected ion recording, and daughter scan mode were used for qualitative analyses. Quantitative PA analyses were made based on MS/MS MRM as described (51). Briefly, MRM transitions for each individual PA were determined based on PA standards obtained from Avanti Polar Lipids. The PAs were identified as deprotonated parent ions [M-H$^-$], and cone energy was optimized for each PA and set to 44 V. The predominant daughter fragment ions were then used for quantitative MRM analysis. After optimization, the collision energy was set to 44 V. MRM transitions and specific retention times were used to selectively monitor PA. Data acquisition and analysis were performed with the MassLynx software (Version 4.1) running under Windows XP professional on a Pentium PC.

DAG Measurements by LC–MS/MS. Neuron lysates from one six-well plate well (prepared as for PA) and ±80 mg of postmortem human brain samples (males, aged between 57 and 78, with one FXS aged 25) ground in a liquid nitrogen cooled mortar were extracted with 2 mL of chloroform/methanol 2/1 (vol/vol), 1 mL of water, and 10 μL of synthetic internal standard (DAG 15:0/15:0) from Sigma Aldrich, sonicated for 30 s, vortexed, and centrifuged. The lower organic phase was transferred to a new tube, and the upper aqueous phase was reextracted with 2 mL of chloroform. Organic phases were combined and evaporated to dryness under nitrogen. Lipid extracts were resuspended in 50 μL of eluent A, and a synthetic internal lipid standard (DAG 17:0/17:0) from Nu-Check Prep was added. LC-MS/MS (MRM mode) analyses were performed with mass spectrometer model QTRAP 5500 (ABSciex) coupled to a LC system (Ultimate 3000; Dionex). Analyses were achieved in positive mode. Nitrogen was used as curtain gas (set to 20), gas1 (set to 25), and gas2 (set to 0). Needle voltage was at +5,500 V without needle heating; the declustering potential was set at +86 V. The collision gas was also nitrogen; collision energy was adjusted to +34 V. Dwell time was set to 3 ms. Reversed-phase separation was carried out at 30 °C on a Phenomenex Luna 3u C8 column (150 mm × 1 mm, 3-μm particle size, 100-Å pore size). Eluent A was ACN/MeOH/H_2O (19/19/2, vol/vol/vol) +0.2% formic acid +0.028% NH_4OH, and eluent B was isopropanol +0.2% formic acid +0.028% NH_4OH. The gradient elution program was 0–5 min, 15% (vol/vol) B; 5–35 min, 15–40% B; 35–40 min, 80% B; and 40–55 min, 15% B. The flow rate was 40 μL/min, and 3-μL sample volumes were injected. The relative levels of DAG species were determined by measuring the area under the peak, determined by using

MultiQuant software (Version 2.1; ABSciex) and normalizing to the area of the DAG internal standard.

AAV Vector Construction. A shRNA designed to target *Dgkκ* (shRNA *Dgkκ* 5′-GGAATGCACTACTGGTATTCC) and the selected shRNA–*scramble* sequence (5′-GCGCTTAGCTGTAGGATTC) that has no match in silico in the mouse genome were cloned under the control of the mU6 promoter into a pAAV-MCS–derived plasmid expressing enhanced green fluorescent protein (EGFP) under the control of a CMV promoter. Overexpression of *Dgkκ* was achieved by cloning HA-tagged *Dgkκ* under the control of the hSynapsin promoter replacing EGFP in the control plasmid pENN.AAV.hSynapsin.EGFP.RBG (provided by the Penn Vector Core at University of Pennsylvania, Philadelphia). Recombinant adeno-associated virus serotype 9 (AAV9) coexpressing EGFP and shRNA (AAV9-EGFP-shRNA-*Dgkκ* and control AAV9-EGFP-shRNA-*scramble*), as well as AAV9 expressing HA-*Dgkκ* or EGFP (AAV9-hSyn-HA-*Dgkκ* and control AAV9-hSyn-EGFP) were generated. AAV production was carried out by using the AAV Helper-Free system (Agilent Technologies) with some modifications. AAV9 vectors were generated by triple transfection of 293T/17 cell line using either pAAV-EGFP-shRNA-*Dgkκ or* pAAV-EGFP-shRNA-*scramble,* pAAV-hsynapsin-HA-*Dgkκ* or pENN.AAV.hSynapsin.EGFP.RBG together with pAAV2/9 (Penn Vector Core) containing cap genes of AAV serotype 9 and pHelper. Two days after transfection, cells were collected, lysed by three freeze/thaw cycles in dry ice-ethanol and 37 °C baths, further treated with 100 U/mL Benzonase (Novagen) for 30 min at 37 °C, and clarified by centrifugation. Viral vectors were purified by iodixanol (Optiprep; Axis Shield) gradient ultracentrifugation followed by dialysis and concentration against PBS containing 0.5 mM MgCl2 using centrifugal filters (Amicon Ultra-15 100 K). Viral particles were quantified by real-time PCR using a linearized standard plasmid pAAV-EGFP. To achieve comparable working concentrations, viruses were diluted to a final concentration of 5×10^{12} viral genomes per mL and stored at −80 °C until use.

Slice Culture Transfection and Imaging. Hippocampal organotypic slice cultures (400-μm thick) were prepared from postnatal 5- to 6-d-old C57BL/6 *Fmr1*$^{+/y}$ or its *Fmr1*$^{-/y}$ littermate mice by using a protocol approved by the Geneva veterinary office and maintained under culture conditions as described (52). Transfection was carried out at 7 DIV with a biolistic method (Helios Gene Gun; Bio-Rad) using gold beads coated with mRFP and either pAAV-EGFP-shRNA-*Dgkκ*, pAAV-EGFP-shRNA-*scramble*, pAAV-hSynapsin-EGFP, or pAAV-hSynapsin-Dgkκ. Repetitive confocal imaging was performed as described (52). Briefly, dendritic segments of CA1 transfected neurons (30–40 μm in length) were imaged from 12 to 15 DIV (at 0, 5, 24, 48, and 72 h) by using an Olympus Fluoview 300 system, and analysis of the Z-stacked images obtained was performed by using Osirix software.

Slice Infection and Electrophysiology. To investigate the functional role of Dgkκ, the CA1 area of hippocampal organotypic slices was infected at 4 DIV by placing a small piece of porous membrane on top of the CA1 area (White FHLC Membrane, Filter type 0.45 μm; EMD Millipore) injected with 0.3 μL (5×10^{12} viral genomes per mL) of either AAV9-EGFP-shRNA-*Dgkκ* or AAV-EGFP-shRNA-*scramble* viruses. The injection of the porous membrane was carried out by using a picospritzer (Toohey). The porous membrane was removed after 1 h and the slices maintained under culture conditions. The efficacy of infection was verified in all slices before the electrophysiological recordings by checking the level and area of expression of GFP. Infected slice cultures were tested electrophysiologically at DIV 7–8 for LTD and DIV14–15 for LTP and placed in an interface-type of recording chamber and continuously perfused with a medium containing (in mM): NaCl 124, KCl 1.6, $CaCl_2$ 2.5, $MgCl_2$ 1.5, $NaHCO_3$ 24, KH_2PO_4 1.2, glucose 10, and ascorbic acid 2; saturated with 95% O2 and 5% CO_2 (pH 7.4; temperature 31 °C). EPSPs were evoked by stimulation of a group of CA3 cells by using a stimulating electrode made of twisted nichrome wires, and responses were recorded in the CA1 stratum region by using a glass patch pipette. LTD was induced by a low-frequency stimulation protocol (900 pulses at 5 Hz), whereas LTP was induced by TBS (3×5 bursts at 5 Hz composed each of four pulses at 100 Hz) as in ref. 53. EPSPs were recorded by using IGOR software, and variations in response size were assessed by measuring EPSP slopes and expressed as percent of baseline values.

Stereotaxic Surgery and AAV Injections. Mice (C57BL/6J) were deeply anesthetized with ketamine/xylazine (Virbac/Bayer, 100/10 mg/kg, 10 mL/kg, intraperitoneal) dissolved in sterile isotonic saline (NaCl 0.9%) and mounted onto a stereotaxic frame (Unimecanique). AAV9-EGFP-shRNA-*Dgkκ* or AAV-EGFP-shRNA-*scramble* (5×10^{12} viral genomes per mL) was injected bilaterally into the striatum (coordinates relative to bregma: anterior-posterior + 0.7 mm; lateral = ±1.5 mm; vertical −4.5 mm) according to the mouse brain atlas (56). A volume of 1.5 μL of AAV vectors per site of injection was delivered bilaterally with a slow injection rate (0.1 μL/min) through a 30-gauge stainless steel cannula connected to an infusion pump. After each injection was completed, the injector was left in place for an additional 10 min to ensure optimal diffusion and minimize backflow while withdrawing the injector. Behavioral experiments were conducted 4 wk after AAV injections to allow sufficient time for viral transduction and Dgkκ expression. Effective gene knockdown was assessed by qRT-PCR (Fig. S3*D*).

ACKNOWLEDGMENTS. We thank F. Bellereau, R. Hattenberger, A. Bruetsch, I. Marti Fernandez, S. Pannetier, A. Geoffroy, V. Fraulob, and T. Maurin for technical assistance; E. Bechara for help with the CLIP approach; F. Sakane for materials; C. Thibault for advice with microarray strategy; M. Gendron for mice care; and K. Hnia, N. Charlet-Berguerand, and O. Manzoni for helpful discussions. The DAG analyses were performed at the Metabolome Facility-MetaboHUB (ANR-11-INBS-0010). This work was supported by ANR Grant ANR-12-BSV8-0022 and Fondation Jérôme Lejeune funding (to H.M.), College de France and USIAS (J.-L.M.), and APLM (R.T.). This study was also supported by ANR-10-LABX-0030-INRT, a French State fund managed by the ANR under the frame program Investissements d'Avenir ANR-10-IDEX-0002-02.

1. Nelson DL, Orr HT, Warren ST (2013) The unstable repeats–Three evolving faces of neurological disease. *Neuron* 77(5):825–843.
2. Santoro MR, Bray SM, Warren ST (2012) Molecular mechanisms of fragile X syndrome: A twenty-year perspective. *Annu Rev Pathol* 7:219–245.
3. Michalon A, et al. (2012) Chronic pharmacological mGlu5 inhibition corrects fragile X in adult mice. *Neuron* 74(1):49–56.
4. Khandjian EW, Corbin F, Woerly S, Rousseau F (1996) The fragile X mental retardation protein is associated with ribosomes. *Nat Genet* 12(1):91–93.
5. Huber KM, Gallagher SM, Warren ST, Bear MF (2002) Altered synaptic plasticity in a mouse model of fragile X mental retardation. *Proc Natl Acad Sci USA* 99(11): 7746–7750.
6. Sidorov MS, Auerbach BD, Bear MF (2013) Fragile X mental retardation protein and synaptic plasticity. *Mol Brain* 6:15.
7. Darnell JC, Klann E (2013) The translation of translational control by FMRP: Therapeutic targets for FXS. *Nat Neurosci* 16(11):1530–1536.
8. Qin M, Kang J, Burlin TV, Jiang C, Smith CB (2005) Postadolescent changes in regional cerebral protein synthesis: An in vivo study in the FMR1 null mouse. *J Neurosci* 25(20): 5087–5095.
9. Brown V, et al. (2001) Microarray identification of FMRP-associated brain mRNAs and altered mRNA translational profiles in fragile X syndrome. *Cell* 107(4):477–487.
10. Miyashiro KY, et al. (2003) RNA cargoes associating with FMRP reveal deficits in cellular functioning in Fmr1 null mice. *Neuron* 37(3):417–431.
11. Darnell JC, et al. (2011) FMRP stalls ribosomal translocation on mRNAs linked to synaptic function and autism. *Cell* 146(2):247–261.
12. Ascano M, Jr, et al. (2012) FMRP targets distinct mRNA sequence elements to regulate protein expression. *Nature* 492(7429):382–386.
13. Suhl JA, Chopra P, Anderson BR, Bassell GJ, Warren ST (2014) Analysis of FMRP mRNA target datasets reveals highly associated mRNAs mediated by G-quadruplex structures formed via clustered WGGA sequences. *Hum Mol Genet* 23(20):5479–5491.
14. Chen E, Sharma MR, Shi X, Agrawal RK, Joseph S (2014) Fragile X mental retardation protein regulates translation by binding directly to the ribosome. *Mol Cell* 54(3): 407–417.
15. Ule J, et al. (2003) CLIP identifies Nova-regulated RNA networks in the brain. *Science* 302(5648):1212–1215.
16. Schaeffer C, et al. (2001) The fragile X mental retardation protein binds specifically to its mRNA via a purine quartet motif. *EMBO J* 20(17):4803–4813.
17. Brindley DN, Waggoner DW (1996) Phosphatidate phosphohydrolase and signal transduction. *Chem Phys Lipids* 80(1-2):45–57.
18. Conn PJ, Pin JP (1997) Pharmacology and functions of metabotropic glutamate receptors. *Annu Rev Pharmacol Toxicol* 37:205–237.
19. de Chaffoy de Courcelles D, et al. (1989) The role of endogenously formed diacylglycerol in the propagation and termination of platelet activation. A biochemical and functional analysis using the novel diacylglycerol kinase inhibitor, R 59 949. *J Biol Chem* 264(6):3274–3285.
20. Koekkoek SK, et al. (2005) Deletion of FMR1 in Purkinje cells enhances parallel fiber LTD, enlarges spines, and attenuates cerebellar eyelid conditioning in Fragile X syndrome. *Neuron* 47(3):339–352.
21. Hu H, et al. (2008) Ras signaling mechanisms underlying impaired GluR1-dependent plasticity associated with fragile X syndrome. *J Neurosci* 28(31):7847–7862.
22. Lauterborn JC, et al. (2007) Brain-derived neurotrophic factor rescues synaptic plasticity in a mouse model of fragile X syndrome. *J Neurosci* 27(40):10685–10694.
23. Gunaydin LA, et al. (2014) Natural neural projection dynamics underlying social behavior. *Cell* 157(7):1535–1551.
24. Rothwell PE, et al. (2014) Autism-associated neuroligin-3 mutations commonly impair striatal circuits to boost repetitive behaviors. *Cell* 158(1):198–212.
25. Dahlhaus R, El-Husseini A (2010) Altered neuroligin expression is involved in social deficits in a mouse model of the fragile X syndrome. *Behav Brain Res* 208(1):96–105.
26. Mineur YS, Huynh LX, Crusio WE (2006) Social behavior deficits in the Fmr1 mutant mouse. *Behav Brain Res* 168(1):172–175.

27. Pietropaolo S, Guilleminot A, Martin B, D'Amato FR, Crusio WE (2011) Genetic-background modulation of core and variable autistic-like symptoms in Fmr1 knock-out mice. *PLoS One* 6(2):e17073.
28. Spencer CM, et al. (2011) Modifying behavioral phenotypes in Fmr1KO mice: Genetic background differences reveal autistic-like responses. *Autism Res* 4(1):40–56.
29. Comery TA, et al. (1997) Abnormal dendritic spines in fragile X knockout mice: Maturation and pruning deficits. *Proc Natl Acad Sci USA* 94(10):5401–5404.
30. He CX, Portera-Cailliau C (2013) The trouble with spines in fragile X syndrome: Density, maturity and plasticity. *Neuroscience* 251:120–128.
31. Imai S, Kai M, Yasuda S, Kanoh H, Sakane F (2005) Identification and characterization of a novel human type II diacylglycerol kinase, DGK kappa. *J Biol Chem* 280(48): 39870–39881.
32. Vasudevan S, Steitz JA (2007) AU-rich-element-mediated upregulation of translation by FXR1 and Argonaute 2. *Cell* 128(6):1105–1118.
33. Kim K, et al. (2009) Synaptic removal of diacylglycerol by DGKzeta and PSD-95 regulates dendritic spine maintenance. *EMBO J* 28(8):1170–1179.
34. Seo J, et al. (2012) Regulation of hippocampal long-term potentiation and long-term depression by diacylglycerol kinase ζ. *Hippocampus* 22(5):1018–1026.
35. Shirai Y, et al. (2010) Essential role of neuron-enriched diacylglycerol kinase (DGK), DGKbeta in neurite spine formation, contributing to cognitive function. *PLoS One* 5(7):e11602.
36. Yang J, et al. (2011) DGKι regulates presynaptic release during mGluR-dependent LTD. *EMBO J* 30(1):165–180.
37. Almena M, Mérida I (2011) Shaping up the membrane: Diacylglycerol coordinates spatial orientation of signaling. *Trends Biochem Sci* 36(11):593–603.
38. Hama H, Hara C, Yamaguchi K, Miyawaki A (2004) PKC signaling mediates global enhancement of excitatory synaptogenesis in neurons triggered by local contact with astrocytes. *Neuron* 41(3):405–415.
39. Anwyl R (2009) Metabotropic glutamate receptor-dependent long-term potentiation. *Neuropharmacology* 56(4):735–740.
40. de Diego-Otero Y, et al. (2009) Alpha-tocopherol protects against oxidative stress in the fragile X knockout mouse: An experimental therapeutic approach for the Fmr1 deficiency. *Neuropsychopharmacology* 34(4):1011–1026.
41. Wang X, et al. (1998) The phosphorylation of eukaryotic initiation factor eIF4E in response to phorbol esters, cell stresses, and cytokines is mediated by distinct MAP kinase pathways. *J Biol Chem* 273(16):9373–9377.
42. Rush AM, Wu J, Rowan MJ, Anwyl R (2002) Group I metabotropic glutamate receptor (mGluR)-dependent long-term depression mediated via p38 mitogen-activated protein kinase is inhibited by previous high-frequency stimulation and activation of mGluRs and protein kinase C in the rat dentate gyrus in vitro. *J Neurosci* 22(14): 6121–6128.
43. Sharma A, et al. (2010) Dysregulation of mTOR signaling in fragile X syndrome. *J Neurosci* 30(2):694–702.
44. Osterweil EK, Krueger DD, Reinhold K, Bear MF (2010) Hypersensitivity to mGluR5 and ERK1/2 leads to excessive protein synthesis in the hippocampus of a mouse model of fragile X syndrome. *J Neurosci* 30(46):15616–15627.
45. Kim K, Yang J, Kim E (2010) Diacylglycerol kinases in the regulation of dendritic spines. *J Neurochem* 112(3):577–587.
46. Ishisaka M, Hara H (2014) The roles of diacylglycerol kinases in the central nervous system: Review of genetic studies in mice. *J Pharmacol Sci* 124(3):336–343.
47. Sakai H, Sakane F (2012) Recent progress on type II diacylglycerol kinases: The physiological functions of diacylglycerol kinase δ, η and κ and their involvement in disease. *J Biochem* 152(5):397–406.
48. Mientjes EJ, et al. (2006) The generation of a conditional Fmr1 knock out mouse model to study Fmrp function in vivo. *Neurobiol Dis* 21(3):549–555.
49. Tusher VG, Tibshirani R, Chu G (2001) Significance analysis of microarrays applied to the ionizing radiation response. *Proc Natl Acad Sci USA* 98(9):5116–5121.
50. Bligh EG, Dyer WJ (1959) A rapid method of total lipid extraction and purification. *Can J Biochem Physiol* 37(8):911–917.
51. Shui G, et al. (2010) Characterization of substrate preference for Slc1p and Cst26p in Saccharomyces cerevisiae using lipidomic approaches and an LPAAT activity assay. *PLoS One* 5(8):e11956.
52. De Roo M, Klauser P, Mendez P, Poglia L, Muller D (2008) Activity-dependent PSD formation and stabilization of newly formed spines in hippocampal slice cultures. *Cereb Cortex* 18(1):151–161.
53. Boda B, Mendez P, Boury-Jamot B, Magara F, Muller D (2014) Reversal of activity-mediated spine dynamics and learning impairment in a mouse model of Fragile X syndrome. *Eur J Neurosci* 39(7):1130–1137.
54. Subramanian M, et al. (2011) G-quadruplex RNA structure as a signal for neurite mRNA targeting. *EMBO Rep* 12(7):697–704.
55. Krezel W, et al. (1998) Impaired locomotion and dopamine signaling in retinoid receptor mutant mice. *Science* 279(5352):863–867.
56. Paxinos G, Franklin KBJ (2001) *The Mouse Brain in Stereotaxic Coordinates* (Academic, New York).
57. Becker JA, et al. (2014) Autistic-like syndrome in mu opioid receptor null mice is relieved by facilitated mGluR4 activity. *Neuropsychopharmacology* 39(9):2049–2060.
58. Silverman JL, Yang M, Lord C, Crawley JN (2010) Behavioural phenotyping assays for mouse models of autism. *Nat Rev Neurosci* 11(7):490–502.
59. Deacon RM (2006) Assessing nest building in mice. *Nat Protoc* 1(3):1117–1119.
60. Sager TN, et al. (2010) Nest building performance following MPTP toxicity in mice. *Behav Brain Res* 208(2):444–449.
61. Le Merrer J, Rezai X, Scherrer G, Becker JA, Kieffer BL (2013) Impaired hippocampus-dependent and facilitated striatum-dependent behaviors in mice lacking the δ opioid receptor. *Neuropsychopharmacology* 38(6):1050–1059.